applied sciences

MDPI

Article

Experimental Analysis of Water Pressure and Temperature Influence on Atomization and Evolution of a Port Water Injection Spray

Lucio Postrioti [1,*], Gabriele Brizi [2] and Gian Marco Finori [1]

[1] Department of Engineering, University of Perugia, 06125 Perugia, Italy; gianmarco.finori@studenti.unipg.it
[2] STSe srl, 06125 Perugia, Italy; gabriele.brizi@stse.eu
* Correspondence: lucio.postrioti@unipg.it; Tel.: +39-075-5853733

Abstract: Port water injection (PWI) is considered one of the most promising technologies to actively control the increased knock tendency of modern gasoline direct injection (GDI) engines, which are rapidly evolving with the adoption of high compression ratios and increased brake mean effective pressure levels in the effort to improve their thermal efficiency. For PWI technology, appropriately matching the spray evolution and the intake system design along with obtaining a high spray atomization quality, are crucial tasks for promoting water evaporation so as to effectively cool down the air charge with moderate water consumption and lubricant dilution drawbacks. In the present paper, a detailed experimental analysis of a low-pressure water spray is presented, covering a lack of experimental data on automotive PWI systems. Phase doppler anemometry and fast-shutter spray imaging allowed us to investigate the influence exerted by the injection pressure level and by the water temperature on spray drop size and global shape, obtaining a complete database to be used for the optimization of PWI systems. The obtained results evidence how significant benefits in terms of atomization quality can be obtained by adopting injection pressure and water temperature levels compliant with standard low injection pressure technologies.

Keywords: water injection; phase doppler anemometry; knock control

Citation: Postrioti, L.; Brizi, G.; Finori, G.M. Experimental Analysis of Water Pressure and Temperature Influence on Atomization and Evolution of a Port Water Injection Spray. *Appl. Sci.* **2021**, *11*, 5980. https://doi.org/10.3390/app11135980

Academic Editor: Cinzia Tornatore

Received: 31 May 2021
Accepted: 21 June 2021
Published: 27 June 2021

1. Introduction

The environmental impact, in terms of global greenhouse effect and pollutant emissions, of the automotive sector is considerable. Hence, severe limitations are in force and designed for, in particular, the adoption of challenging CO_2 emission targets for the next few years [1–3]. Consequently, the automotive industry is quickly adopting innovative technologies, globally aiming for a rapid increase in automotive powertrain efficiency. The leading method followed to improve powertrain efficiency is electrification, with the adoption of a progressively more significant energy storage capacity and electric propulsion system power. The final stage of this evolution is foreseen to be the battery electric vehicle, which ensures a zero CO_2 local emission operation. In this scenario, the internal combustion engine will still play a significant role for many years [4] due to the complexities and costs related to the actual implementation of the electrification path. Accordingly, along with electrification, a significant evolution of the gasoline engine to improve its efficiency is mandatory. The widespread adoption of gasoline direct injection (GDI) in spray-guided or pre-chamber configurations, turbocharging coupled with downsizing and downspeeding, higher compression ratios and application of the Miller cycle seem to be the most interesting innovation lines [5,6]. Unfortunately, many of the aforementioned technologies cause a drastic increase in the knocking tendency due to the increased charge temperature before and during combustion, thus restraining the potential benefits in terms of engine efficiency. As a matter of fact, particularly for high-performance engines, the knock tendency in high load conditions is currently controlled by reducing the spark advance and by enriching

the fuel/air mixture, resulting in an efficiency penalty and in a restriction of the catalyst operating area with an increase of CO_2, CO and HC emissions.

In this frame, water injection technology can be used as an alternative way to control the charge temperature at the end of the intake process and during the combustion phase, thus reducing the risk of abnormal combustion in downsized and highly boosted GDI engines. Water injection can potentially enable $\lambda = 1$ operation in high-load and high-speed operation, even adopting high compression ratios [7–17], thereby gaining significant benefits in terms of engine efficiency while preserving the after-treatment system efficacy in controlling exhaust emissions.

Water injection can be implemented as low-pressure injection in the intake runners (PWI), as high-pressure injection in the combustion chamber (DWI) or as direct injection of a water/gasoline emulsion. Along with the potential benefits in terms of air charge temperature control, clearly water injection has different potential drawbacks, such as a possible lubricant dilution due to the liquid's impact on the cylinder liner. Potentially catastrophic lubricant dilution can be caused by an incorrect match among the spray's global shape with the inlet duct geometry (for PWI systems) or the combustion chamber (for DWI systems) or, in general, by a slow water evaporation rate. Furthermore, the water deposition on the duct and cylinder walls limits the air charge cooling effect, increasing the water flow rate required to effectively control the knock tendency, resulting in water-to-fuel rate ratios in the range of 0.2–0.5 in full load conditions. Among the possible different schemes, port water injection (PWI) is currently considered the most attractive as a compromise between efficacy and cost, being significantly higher for direct water and water/gasoline emulsion injection systems, including the eventual water recovery technologies from the exhaust stream [18].

Since the air charge temperature control potential under water injection is related to the high latent heat of vaporization of the water, the injected water evaporation rate is a crucial factor to be considered in PWI systems' design. In order to promote water evaporation, an adequate match of the water spray characteristics with the intake system design is required, and hence, a detailed knowledge of the spray characteristics is mandatory. In particular, given the moderate air charge temperature (typically in the range of 40–60 °C for intercooled engines) and the short spray residence time in the inlet runner, the water spray atomization quality is crucial for obtaining complete evaporation.

Unfortunately, in the technical literature, there is a substantial lack of detailed experimental data about low-pressure water sprays' global evolution and atomization level to support PWI system design and CFD simulation. In [9], Iacobacci et al. investigated the potential of a PWI system based on PFI injectors supplied with water at 25 °C (P_{inj} = 4 bar,g), changing the water/fuel ratio to mitigate the knock tendency at full load. Cordier et al. [10] tested different water injection technologies on a single-cylinder research engine, obtaining significant efficiency improvements. For the tested PWI configuration, P_{inj} was varied in the range of 5–20 bar,g, but no details about the resulting spray characteristics were reported. In [12], Paltrinieri et al. experimentally investigated the application of a PWI system operated at P_{inj} = 7 bar,g and T_w = 55 °C for a single-cylinder research engine with water-to-fuel ratios up to 60%. Different injector designs and positions along the inlet duct were used to explore the actuation timing effect. In this analysis, CFD simulations of the water spray evolution in the intake duct were carried out to investigate the spray–air interaction, but the effect of the spray characteristics with different operating conditions was not investigated. In other numerical analyses of water injection systems, the water spray characteristics, or even its evaporation rate, are assumed to be constant or similar to fuel sprays generated at the same injection pressure level [13,15,16].

In the present paper, a detailed experimental analysis of a low-pressure water spray is presented, discussing the effect of both the injection pressure and water temperature in the rail on the jet evolution and size characteristics. According to the current approach of the automotive industry for the definition of a PWI system's architecture, both these parameters were varied in ranges compliant with standard PFI technology to reduce the

complexity and cost of key components such as injectors, rails and sensors. The injection pressure was varied from 5 bar,g to 11 bar,g, covering a pressure range explored by other Authors for PFI injectors [19]. Correspondingly, the water temperature in the rail was changed from 20 °C to 110 °C, approaching flash boiling conditions in order to promote the spray break-up and drop evaporation [20,21]. The analysis was carried out by a phase doppler anemometry (PDA) system and by a fast-shutter imaging apparatus in order to investigate both the drops' size quality and global spray characteristics obtained in a range of operating conditions. In the following sections, the experimental set-up and the test plan will be presented first, and the obtained results will be discussed.

2. Materials and Methods

The PWI injector (Bosch EV14) used for the present analysis was characterized in terms of the mean injected mass, global spray evolution, drop size and velocity. The main characteristics of the tested injector are reported in Table 1. The static flow rate was measured by the dINJ injection analyzer, a Zeuch method-type injection analyzer specifically designed to operate with low-pressure injection systems [8,22].

Table 1. PWI injector characteristics.

Injector	Bosch GS EV14
Holes	4 × 220 µm, symmetric to injector axis
Static Flow Rate	3.5 mm^3/ms @P_{inj} 5 bar,g ; T_w = 20 °C
Injector Driver	Darlington TIP121, V_{supply} 14 V.

The injector under testing was fed with distilled water statically pressurized with nitrogen in the range from 5 bar,g to 11 bar,g (up to 15 bar,g only for the flow tests). Pressurized water was accumulated in a 100-cc reservoir, which was used as rail to directly feed the injector to have negligible pressure fluctuations during the injection event, according to the rules of JSAE2715. The rail structure was used as a fixture for an electric heater used to control water temperature. The feedback thermocouple was installed at the injector inlet in the same position as the Keller PAA M5 HB sensor (20 bar f.s., 50 kHz bandwidth, 1% accuracy) used to monitor the rail pressure. The injector current time history was acquired by a Pico TA189 probe (30 A, 100 kHz bandwidth) and averaged over 30 consecutive injection events. A schematic of the experimental setup is reported in Figure 1.

In each operating condition, the mean injected volume was measured by a precision balance (Radwag PS 1000/C/2, resolution of 1 mg, accuracy ±1.5 mg) during three repetitions of a 3000-shot sequence with a 10 Hz injection frequency.

In previous studies (e.g., [8,23]), the effect of the test vessel's pressure and temperature on low-pressure water sprays was investigated, concluding that the air temperature's variation from ambient to 50–60 °C (typical of boosted conditions with an intercooler) has negligible effects on the spray's evolution and size. On the other hand, boosted pressure levels have the similar effect of a corresponding injection pressure reduction, with the pressure differential across the injector being the main driving force affecting the spray's evolution. As a consequence, in this research, the test vessel's pressure and temperature were maintained at 1 bar,a and 25 °C for all the operating conditions.

In Table 2, the operating conditions used for the flow test are reported, evidencing the imposed water temperature at the injector's inlet.

The global spray evolution was investigated by a fast-shutter imaging technique, applied according to an ensemble averaging approach. The imaging apparatus was based on a pulsed Nd-Yag laser (Litron Nano L 200–20, 200 mJ/shot, shot duration 6 ns), which was used as a light source. The laser was synchronized with a fast-shutter, high-resolution CMOS camera (Dalsa Genie Nano M4020, resolution 3008 × 4112, 12-bit). According to the ensemble averaging approach, only one image per injection event was acquired at a given delay from the injection event's start (the TTL signal enabling the injector driver was used as a trigger). The statistical analysis of the spray's global development at an assigned

delay was carried out by repeating the image acquisition over a series of consecutive injection events (30 in the present work). The repetition of the aforementioned acquisition sequence at different delays from the injection start allowed for characterization of the complete spray development throughout the entire injection event. The acquired images at the different timings were analyzed off-line by means of a proprietary digital analysis procedure developed in the LabVIEW™ environment, obtaining the spray tip penetration curves and global cone angle according to the JSAE2715 prescriptions. More details about the image analysis procedure are reported in [24,25].

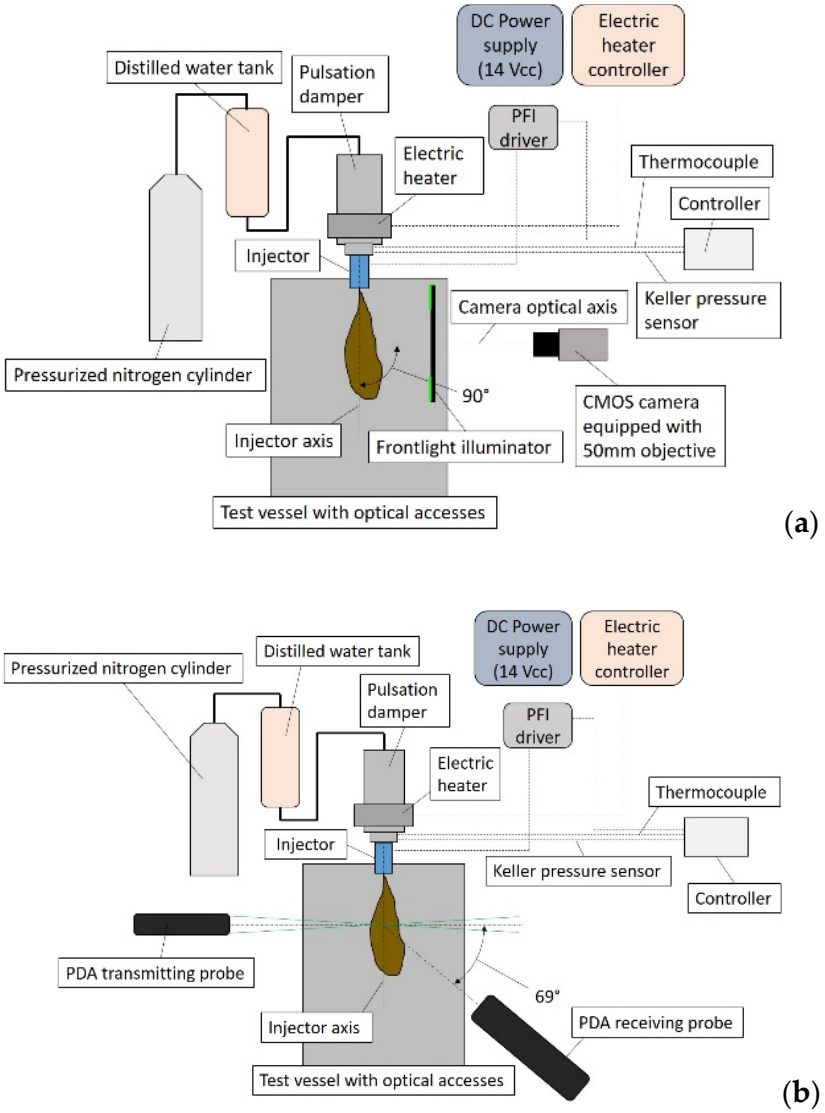

Figure 1. Schematic of the experimental setup for imaging (**a**) and PDA (**b**).

Table 2. Flow test plan showing the water temperature in °C at the injector's inlet.

		Energizing Time (μs)							
		2000	3000	4000	5000	6000	8000		
Injection Pressure (bar,g)	5								
	7								Water Temp. (°C)
	9								
	11							base	20
	15							extended	20, 55, 90, 110

The test plan used for the global spray analysis by imaging was based on a full-factorial analysis of injection pressure P_{inj} levels of 5, 7 and 11 bar,g with water temperature levels of 20, 55, 90 and 110 °C. All spray imaging tests were carried out with an ET of 5 ms in order to ensure adequate steady flow operation for the injector and evidence the effects of both the water temperature and the injection pressure.

The effect of the water temperature and injection pressure on the drop size was evaluated using a phase doppler anemometer (Dantec Dynamics P80) along a measuring traverse composed of 18 stations. The traverse was positioned at Z = 50 mm downstream of the nozzle plate and aligned with the projection of two of the four nozzle holes on the examined plane to evidence the global spray symmetry. In Table 3, the main specifications for the PDA system used for the tests are reported.

Table 3. PDA system specifications.

Transmitter	60 mm
Receiver	HiDense 112 mm
Laser Source	Coherent Genesis MX514
Frequency Shift	40 MHz
Focal length (TX/RX)	310 mm/310 mm
Scattering Angle	110°
Drop Diameter Range	1–400 μm
Drop Velocity Range	−5–30 m/s
Ref. System Origin (X = Y = 0, Z = 0)	Nozzle tip center; Velocity positive: downward

The drop size and velocity characteristics were investigated in the operating conditions reported in Table 4. In all PDA tests, an ET of 5 ms was applied, acquiring data in a 30-ms time window after the start of the ET to capture the entire spray evolution, including its complete tail. Prescriptions from JSAE2715 were followed during the tests in terms of spray boundary detection and minimum number of samples per measuring position. The data were collected during 3000 consecutive shots, operating the injector at 8 Hz in each examined station.

Table 4. PDA test plan, with the water temperature measured at the injector inlet.

		Water Temperature (°C)			
		20	**55**	**90**	**110**
Injection Pressure (bar,g)	5		X		
	7	X	X	X	X
	9		X		
	11		X		

3. Results

3.1. Flow Test Results

In Figure 2, the results obtained in terms of the mean injected quantity, parametrically varying both the injection pressure level from 5 to 15 bar,g and the water temperature at the injector inlet from 20 °C to 110 °C, are reported. On the left in the same figure, the results are reported for when P_{inj} 7 = bar,g was assumed as the reference injection pressure level.

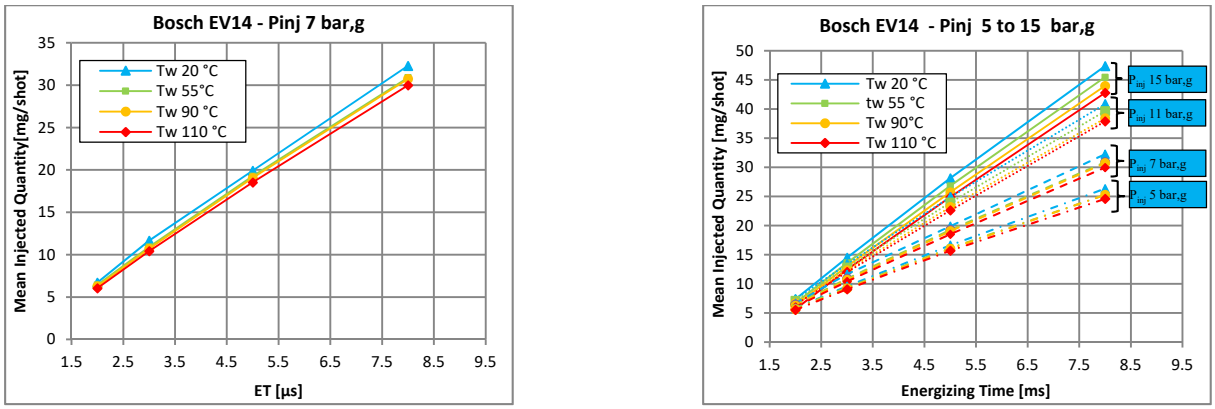

(**a**) (**b**)

Figure 2. Mean injected quantity for T_w range 20–110 °C and P_{inj} = 7 bar,g (**a**) and from 5 to 15 bar,g (**b**).

From the obtained results, the effect of the water temperature increasing on the injected mass is evident. For a given injection pressure level, the higher the fluid temperature, the lower the injected quantity. With the ET at 5 ms and the water temperature changing from 20 °C to 110 °C, the mass percentage difference ranged from 5.7 % at P_{inj} = 7 bar,g to 11.5% at P_{inj} = 15 bar,g. This is likely to be ascribed mainly to the reduced magnetic force exerted by the solenoid on the injector needle, caused by the increased coil resistance. As is reported in Figure 3, for the reference injection pressure level, the injector current was significantly reduced in high water temperature conditions. Furthermore, the current time history slope—and presumably the needle rise—was slowed at high water temperatures, as is suggested by the delayed occurrence of the needle's fully raised position, evidenced by the sudden slope change in the current profile around 1.5 ms after the ET started.

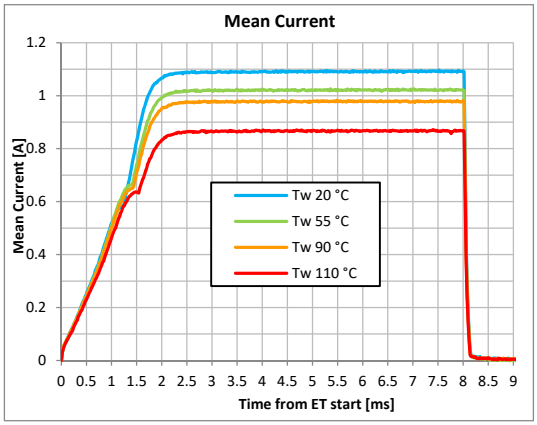

Figure 3. Injector current as a function of the water temperature. P_{inj} = 7 bar,g, and ET = 8.0 ms.

The effect of the fluid's temperature on the injector dynamics was particularly evident for short injection events, during which the injector operated in the so-called "ballistic regime". In ballistic operation, the needle did not attain the fully raised position, and consequently, the flow could not reach a static rate condition. As is reported in Figure 4a, where the flow results are plotted against the injection pressure level (with ET = 2 ms and P_{inj} = 15 bar,g), the injector's opening phase was drastically altered by high water temperature levels. In these conditions, the progressively reduced available magnetic force caused the mean injected mass to be lower at P_{inj} = 11 bar,g (and equal for T_w = 20 °C). Only for ET values longer than 3 ms was the expected rising dependence of the injected mass on P_{inj} obtained, given the presumable attained steady flow conditions and the reduced significance of the needle's opening phase with respect to the entire injection process.

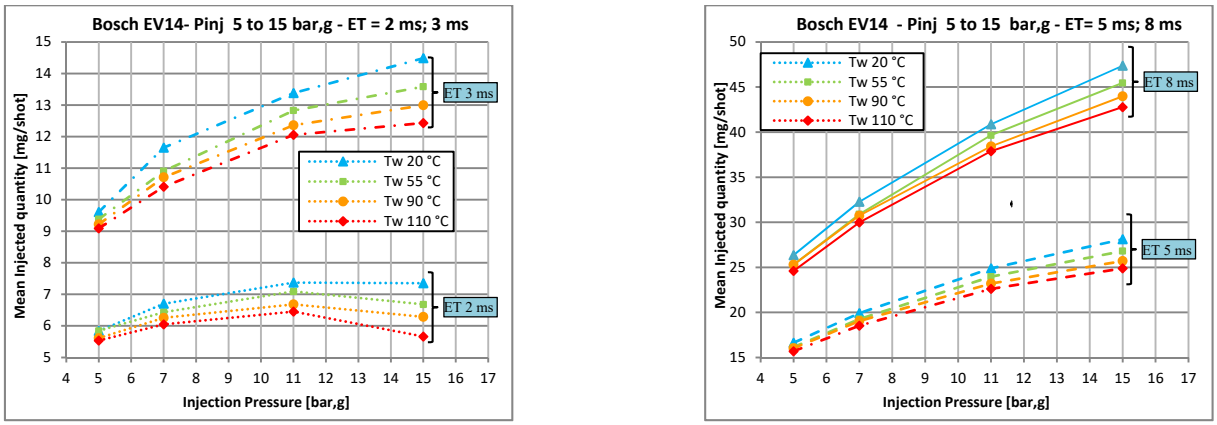

Figure 4. Mean injected quantity vs. injection pressure with water temperatures from 20 °C to 110 °C. (**a**) ET = 2 ms and 3 ms. (**b**) ET = 5 ms and 8 ms.

The obtained flow results seem to suggest that P_{inj} = 15 bar,g is not a feasible operating condition for this injector with a high water temperature and will no longer be investigated in terms of the spray evolution and drop size.

3.2. Spray Global Development

The imaging set-up described in Section 2 was used to investigate the effect of the injection pressure and water temperature on the global spray's evolution. For the sake of brevity, only a short sequence of the spray evolution in the reference condition (P_{inj} = 7 bar,g, 20 °C) is reported in Figure 5 along with pictures of the fully developed spray under high injection pressure and water temperature conditions (Figure 6).

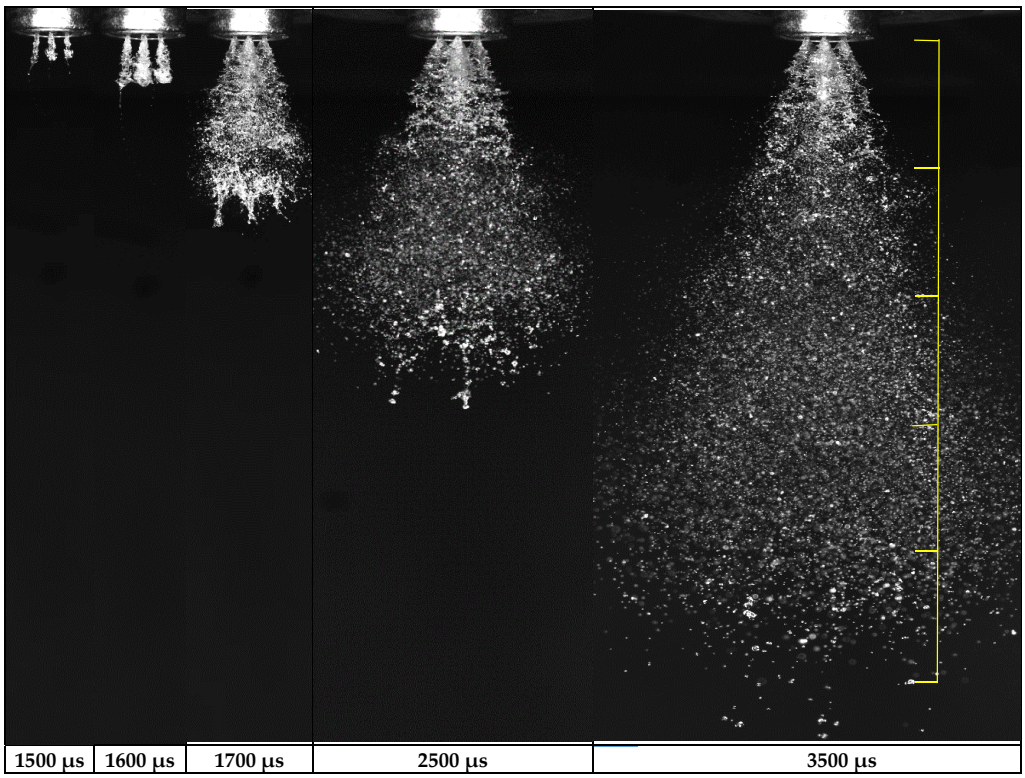

Figure 5. Spray evolution sequence at P_{inj} = 7 bar,g and 20 °C (timing from ET start, scale tick = 10 mm).

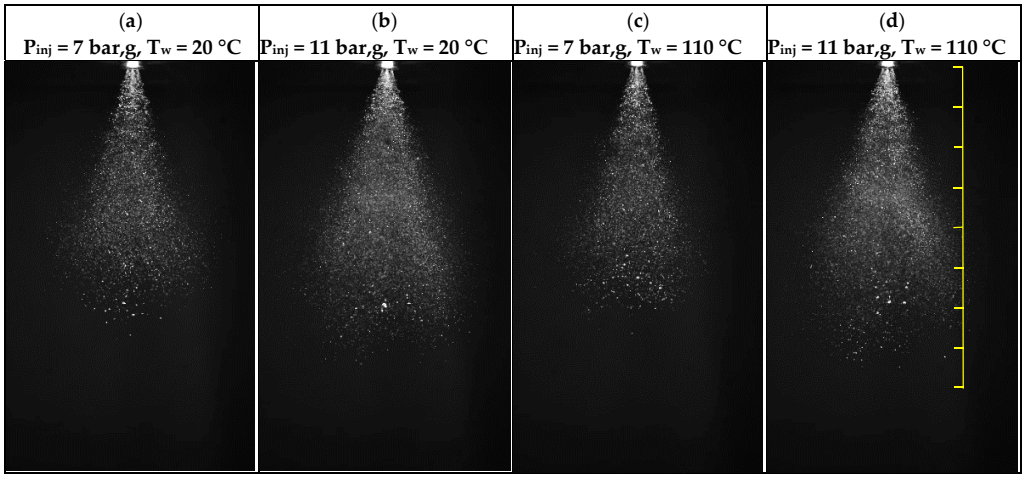

Figure 6. Fully developed spray at 4 ms after the ET's start. Scale tick = 10 mm.

As can be observed in Figure 5, four individual conical flow structures emerged from the nozzle at the beginning of the injection process, initially composed of relatively large ligaments. The four structures merged at a distance between 5 and 10 mm from the injector nozzle. After a short transition zone, at a 10-mm distance downstream, the primary break-up process seemed to be completed. The spray structure hereafter appears to be quite uniform and composed of relatively small drops; only in the most advanced and central part of the spray was the presence of significantly large ligaments clearly perceivable, probably originating from the initial injection transient when the flow velocity was restrained by the needle.

When the operating conditions were changed by increasing the injection pressure from 7 to 11 bar,g (Figure 6a,b), the spray structure was evidently altered, with an increased penetration and cone angle. Furthermore, the spray structure appeared to be composed of smaller droplets, with a reduced presence of large ligaments in the spray's bulk. Only in the spray tip were some large blobs originating from the injector's opening transient still present.

Conversely, the increase in water temperature (Figure 6c,d) did not seem to produce dramatic changes in the spray's overall structure with respect to the corresponding low-temperature operating condition. This evidence seems to suggest that in the tested operating conditions, flash boiling was not triggered despite the high temperature level at the injector inlet, possibly due to the progressive cooling of the water inside the injector body.

The complete set of results in terms of the spray tip penetration and spray cone angle are reported in Figures 7 and 8 for the 12 examined operating conditions, evidencing the effect on the spray's global development of the injection pressure and water temperature, respectively.

As reported in Figure 7, the injection pressure had a significant effect on both the spray tip penetration and global cone angle for all the examined water temperature levels. Globally, 5 ms after the ET's start, changing the injection pressure from P_{inj} = 5 bar,g to P_{inj} = 11 bar,g led the spray tip penetration to increase by 11% at T_w = 20 °C and by 12% at T_w = 110 °C. The spray tip penetration slightly increased from 5 bar,g to 7 bar,g, with this trend being more evident in the final part of the spray evolution and at a higher water temperature. When the injection pressure was raised to 11 bar,g, the final penetration increase was more evident, despite the relatively high injection pressure tending to slow the injector opening transient, consequently leading to the initial spray tip velocity being smaller. As a result, the spray penetration for P_{inj} = 11 bar,g was smaller than for P_{inj} = 7 bar,g up to 1.5 ms after the ET's start, in which time the initial penetration gap was recovered. The effect of the injection pressure on the spray cone angle was even more evident; for all the examined water temperature conditions, the spray diffusion angle progressively increased with higher injection pressure levels, obtaining almost parallel trends for this quantity. It

is also interesting to observe how the monotonically decreasing trend for the spray cone angle changed its slope after the injector closure around 5.8 ms after the ET's start.

The effect of the water temperature at the injector inlet on the spray evolution is analyzed in Figure 8. As can be observed, only marginal effects were exerted by the water temperature on the spray's global structure for all the examined injection pressure levels. To be detailed, an unclear tendency was observed in terms of spray penetration for P_{inj} = 5 bar,g, while the effect was negligible for higher injection pressure levels. In terms of the spray cone angle, the increase in water temperature seemed to decrease the spray cone angle up to 90 °C, while a further increase to 110 °C seemed to attenuate or revert the trend. Globally, a moderate effect of the water temperature on the spray evolution was observed.

3.3. Spray Drop Size and Velocity

The PDA raw data for the measuring station corresponding to the injector axis projection on a plane at 50 mm from the nozzle (coordinates of X = Y = 0; Z = 50 mm) are reported in Figure 9a,b for the reference operating condition P_{inj} = 7 bar,g and Tw = 20 °C. In these plots, all the records relevant to 3000 consecutive injection events are reported (blue dots), along with the average values computed in 0.1 ms time bins (red dots). The ET's start was used as a time reference.

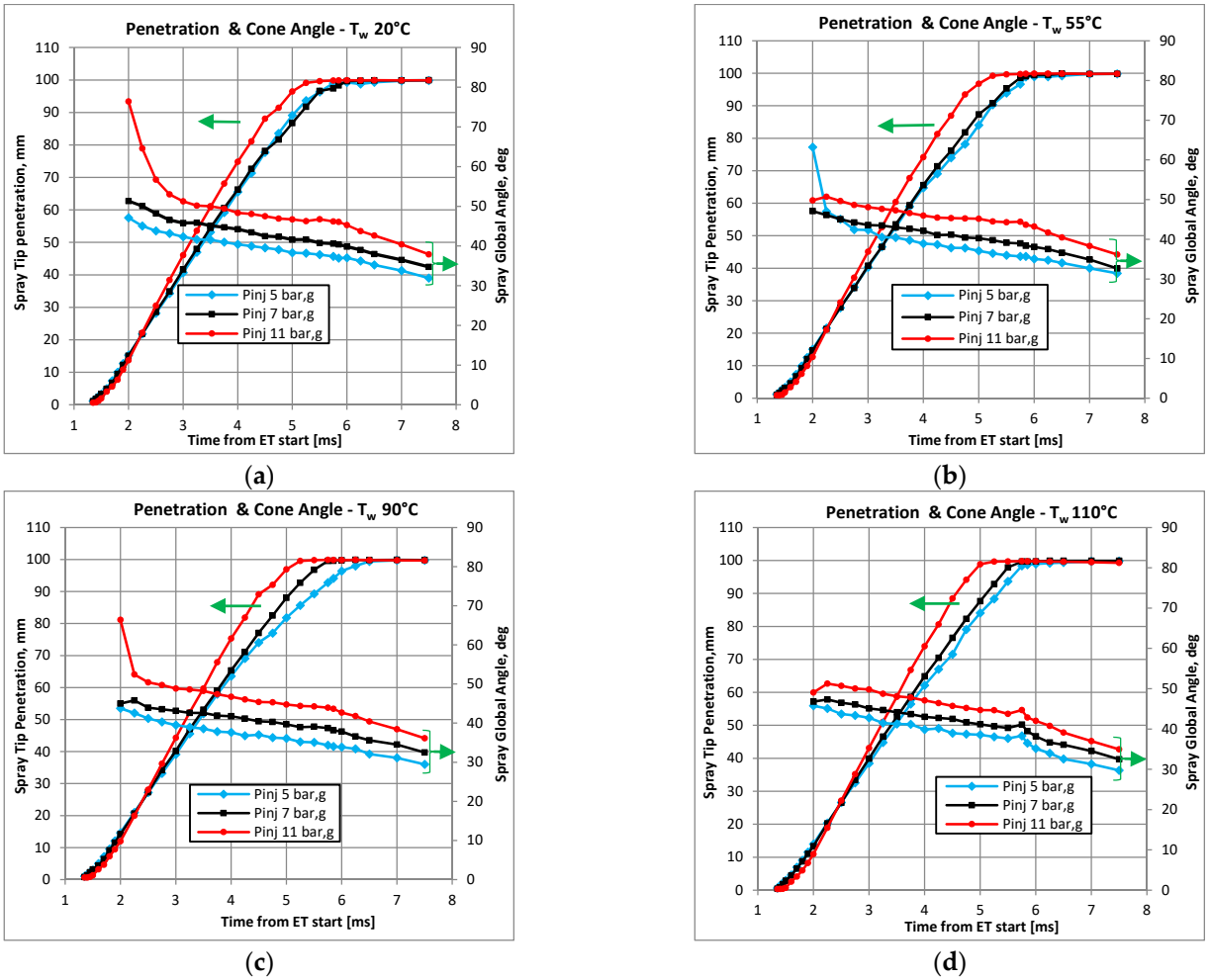

Figure 7. Effect of the injection pressure on the spray tip penetration and cone angle. (**a**) T_W = 20 °C; (**b**) T_W = 55 °C; (**c**) T_W = 90 °C; and (**d**) T_W = 20 °C.

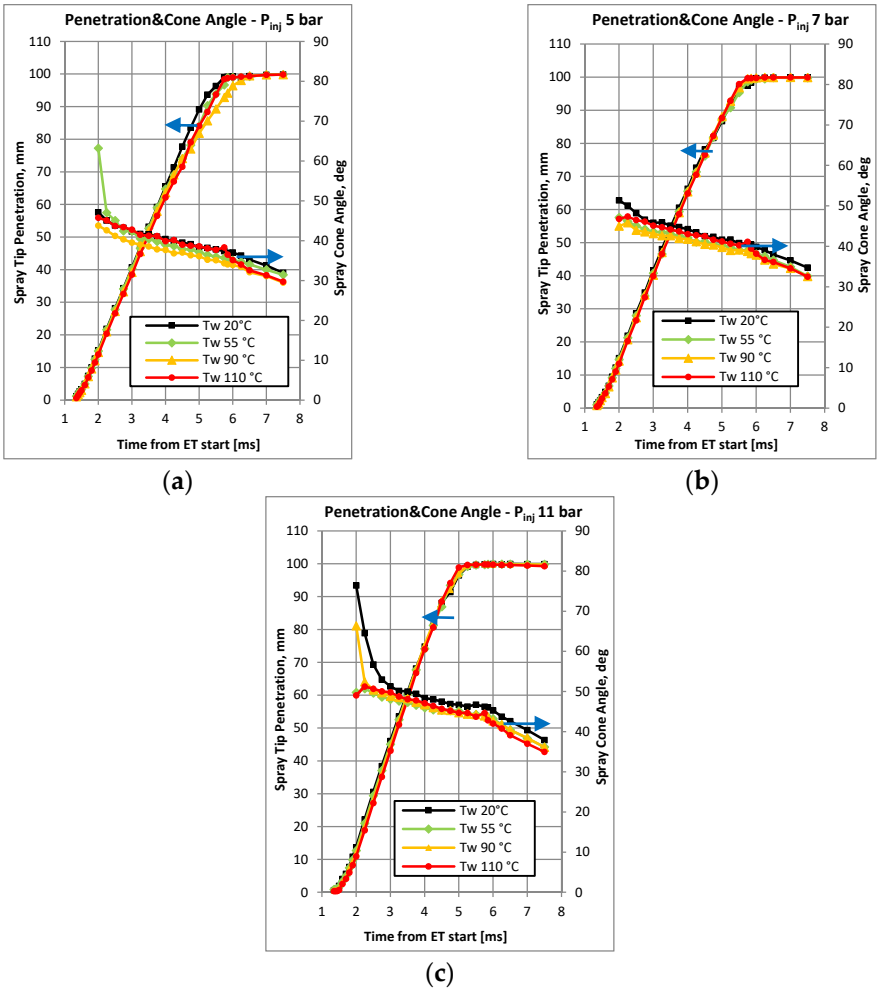

Figure 8. Effect of the water temperature on the spray tip penetration and cone angle. (**a**) P_{inj} = 5 bar,g; (**b**) P_{inj} = 7 bar,g; and (**c**) P_{inj} = 11 bar,g.

As can be seen, the drops' diameters and Z-velocity time histories evidence how the spray approached the considered measuring station about 4 ms after the ET's start. The main part of the spray structure flowed through the considered measuring station between 4 and 8 ms. During this time window, the drops' velocity ranged between approximately 5 and 22 m/s, while the observed drops' diameter range was predominantly between 15 and 150 µm. A significant number of drops with diameters up to 350 µm was also observed, possibly related to the defective primary break-up in the first part of the injection process, as was observed in the spray images. The presence of even such a restricted number of relatively large drops inherently had a non-marginal effect on the resulting Sauter mean diameter.

After 8 ms from the ET's start, the velocity data rapidly decreased to values around 2–3 m/s for the drops pertaining to the spray tail. This part of the spray's structure was composed of very small droplets (diameter values below 40 µm) featuring reduced momentum which continued flowing through the observed position for a long time.

When the injector's water temperature was raised to 110 °C, the drops' velocities and sizes time histories for the same measuring station, reported in Figure 9c,d, were obtained. Marginal effects due to the applied rise in temperature were observed in terms of both the drops' velocities and size ranges for the bulk spray evolution during the 4–8 ms time window, while a significant shift in the mean values was observed below 15 m/s and toward 50 µm.

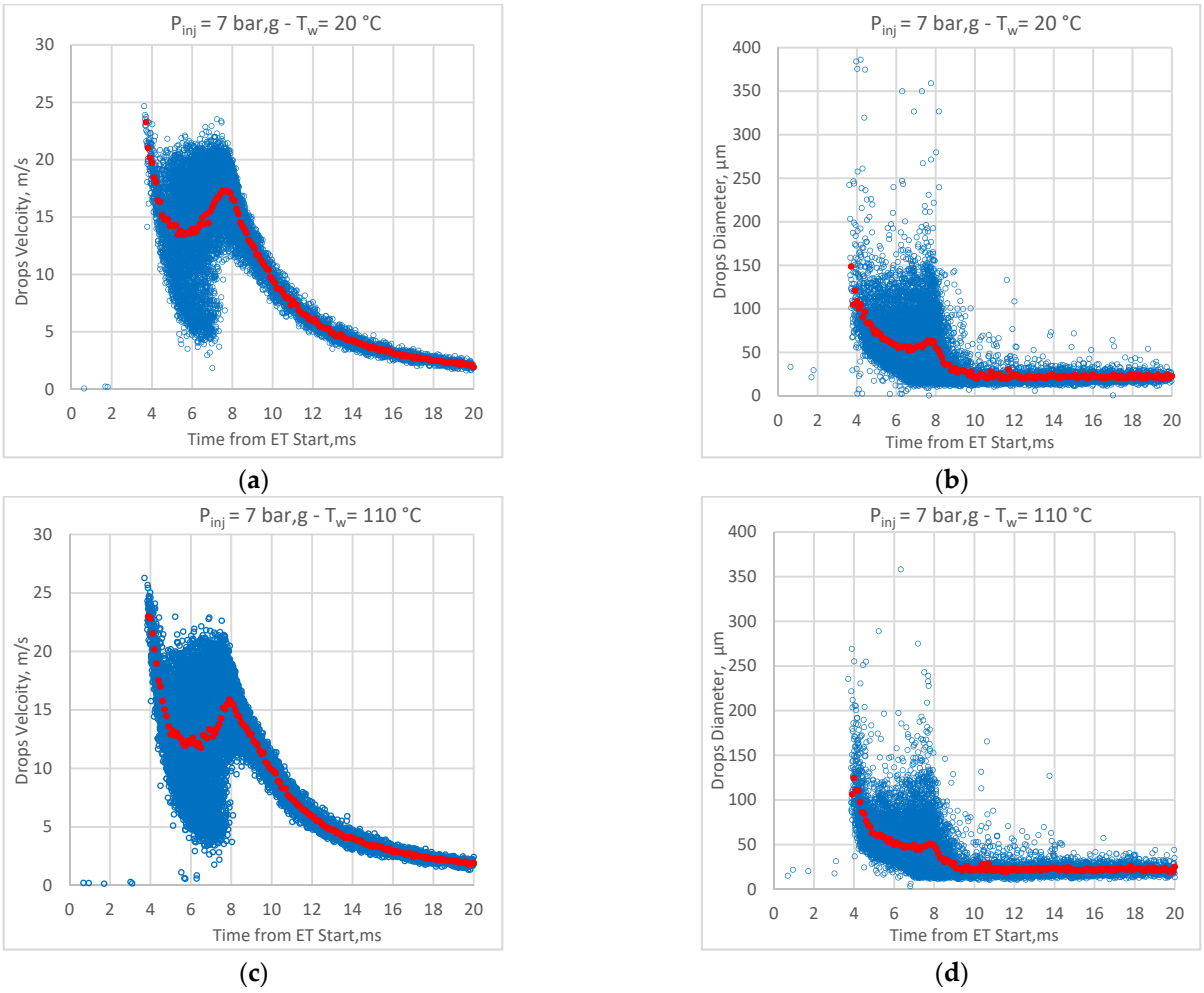

Figure 9. Effect of the water temperature on the drops' sizes and velocities. Raw data in X = Y = 0, Z = 50 mm, P_{inj} = 7 bar,g. (**a**) Drops' velocity for T_w = 20 °C. (**b**) Drops' diameter for T_w = 20 °C. (**c**) Drops' velocity for T_w = 110 °C. (**d**) Drops' diameter for T_w = 110 °C.

In Figure 10, the results obtained with four different water temperature levels at the injector inlet are reported for the complete measuring travers at Z = 50 mm and crossing the entire spray structure. In these plots, both the mean and Sauter mean diameter values are included, along with the mean velocity and relative drop count. All these quantities were computed with data relevant to the entire 30-ms time-window to have a full portrait of the spray quality in the examined positions.

The effect of the water temperature on the drops' sizes, which was already commented on for the X = Y = 0 and Z = 50 mm position, was substantially confirmed for the entire measuring traverse; a significant but not dramatic effect from 20 °C to 110 °C was observed, with size reductions ranging between 8 and 15 µm in terms of the SMD and between 4 and 9 µm in terms of the MD. Minor consequences of raising the water temperature were observed in terms of the drop count and mean velocity, which were proven to change only for the central positions of the spray structure. As was observed when commenting on the spray images in the same operating conditions in Section 3.2, the water temperature's rise at the injector inlet from 20 °C to 110 °C, assumed to be compatible with standard PFI technology (e.g., injector body, rail and pressure sensor), was not adequate to trigger a net flash boiling mechanism for the injection process. Consequently, the injection process resulted in a spray with a basically unaffected shape but appreciably improved atomization quality. Nevertheless, the drops' size improvement was not as significant as was presumably attainable in the case of completely developed flash boiling conditions [25].

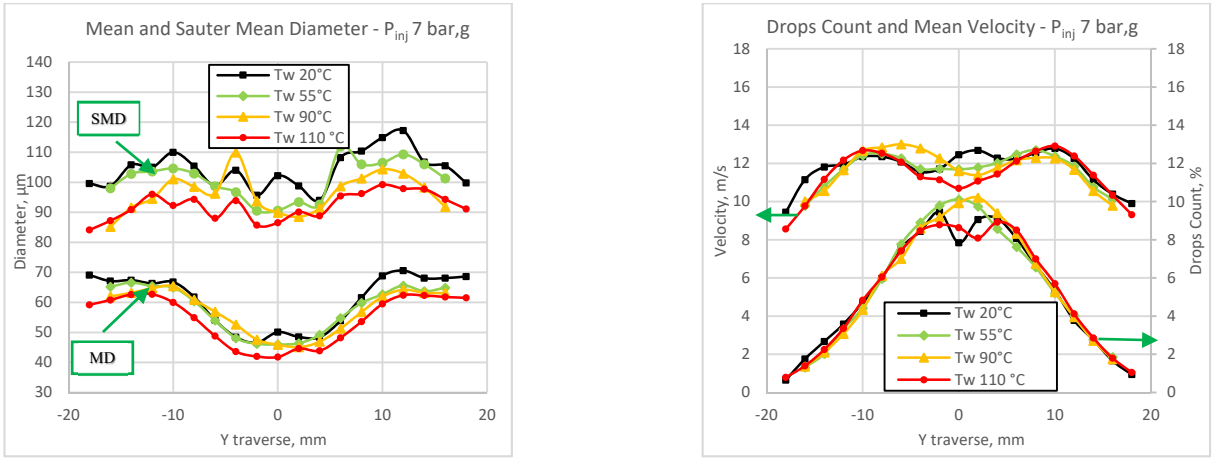

Figure 10. Effect of the water temperature on the drops' sizes and velocities over the measuring traverse at Z = 50 mm. P_{inj} = 7 bar,g. (**a**) Drops' mean diameter. (**b**) Drop count and velocity.

A similar analysis is presented in order to separately analyze the potential effects exerted by an increase of the injection pressure in terms of the spray evolution and atomization quality. In Figures 11 and 12, the results obtained in terms of raw data for the measuring position X = Y = 0 and Z = 50 mm and in terms of the mean for the entire examined traverse are reported.

The injection pressure's effect on the drops' sizes is evident from the comparison of Figure 11b,d, with the P_{inj} = 9 bar,g drop size consistently reduced for the spray bulk (from 4 to 8 ms) for time bin mean values close to 50 µm for a large part of the considered time window. Higher values were observed only for the very initial part of the injection process and around 7 ms when, presumably, the drops produced during the injector's closing phase approached the measuring station. Both the initial and final transients were characterized by a severe channel flow restriction, with consistent flow velocity reduction and drops breaking up the process penalization. For P_{inj} = 5 bar,g, relatively large drops were attained at the Z = 50 mm measuring station with an almost constant velocity during the bulk spray time window, suggesting a moderate drag effect by the surrounding air. Conversely, with the higher injection pressure, the mean drops' velocities showed initially lower values, possibly due to a consistent drag exerted on the finely atomized drops, with the mean velocity rising only later when, presumably, the core of the completely developed spray attained the measuring station.

The analysis in Figure 12 confirmed the significant effect exerted by the injection pressure on drops' characteristics. The pressure increase from 5 to 11 bar,g caused a reduction of the SMD in excess of 20 µm in several stations, with minor effects in the spray's periphery. Smaller and more uniform effects were observed in terms of the mean diameter. The drops' mean velocities consistently increased for all the measuring stations as a direct consequence of the injection pressure's increase. As was observed in Figure 11, the velocity increase was observed mainly in the second part of the 4–8 ms time windows, when the fully developed spray crossed the measuring station. It is also interesting observing how, with P_{inj} = 5 bar,g, the drop count profile was clearly asymmetrical, suggesting incipient off-design operation for the used injector. Correspondingly, the drops' atomization quality in the low-count region was particularly poor.

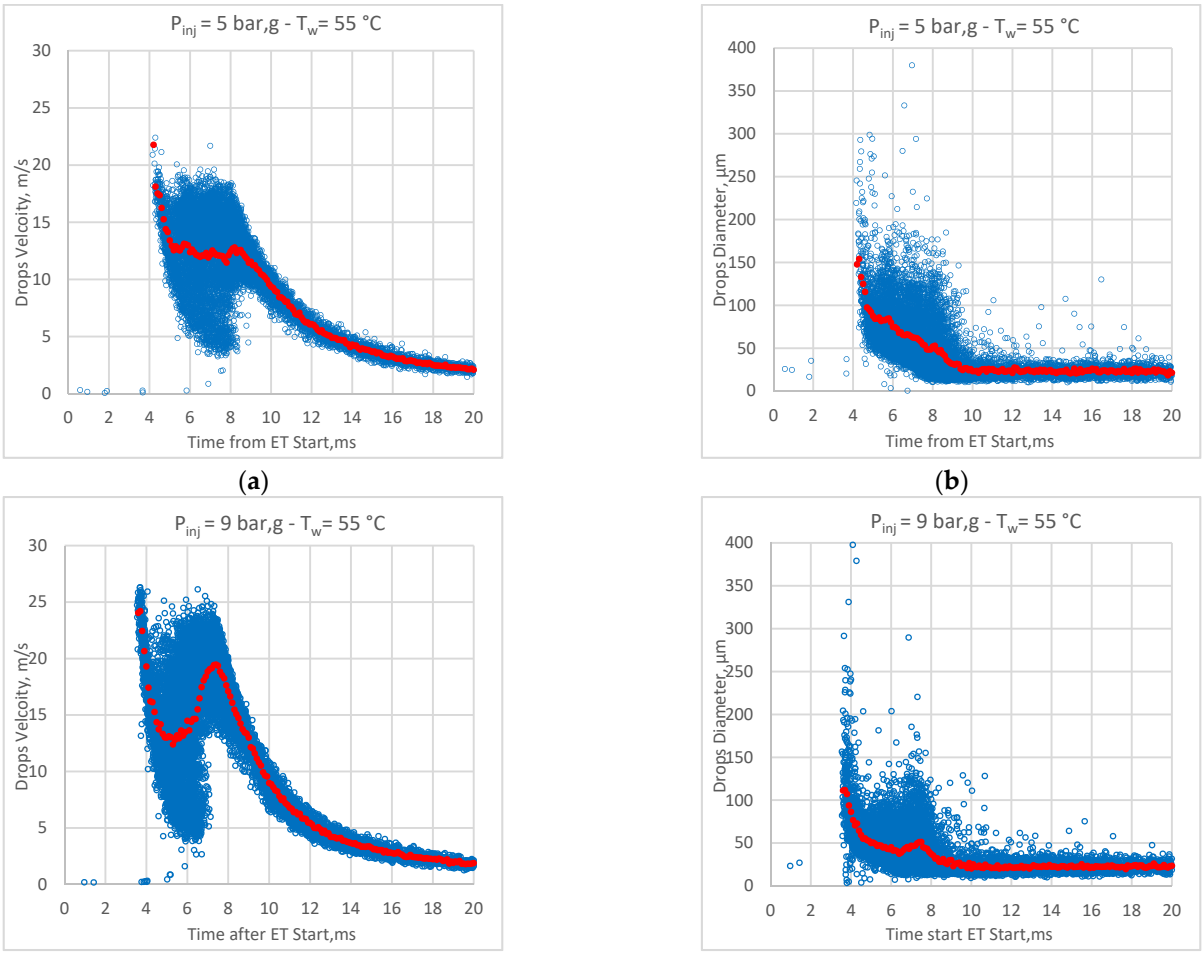

Figure 11. Effect of the injection pressure drops' sizes and velocities. Raw data in X = Y = 0, Z = 50 mm; T_w = 55 °C. (**a**) Drops' velocity for P_{inj} = 5 bar,g. (**b**) Drops' diameter for P_{inj} = 5 bar,g. (**c**) Drops' velocity for P_{inj} = 9 bar,g. (**d**) Drops' diameter for P_{inj} = 9 bar,g.

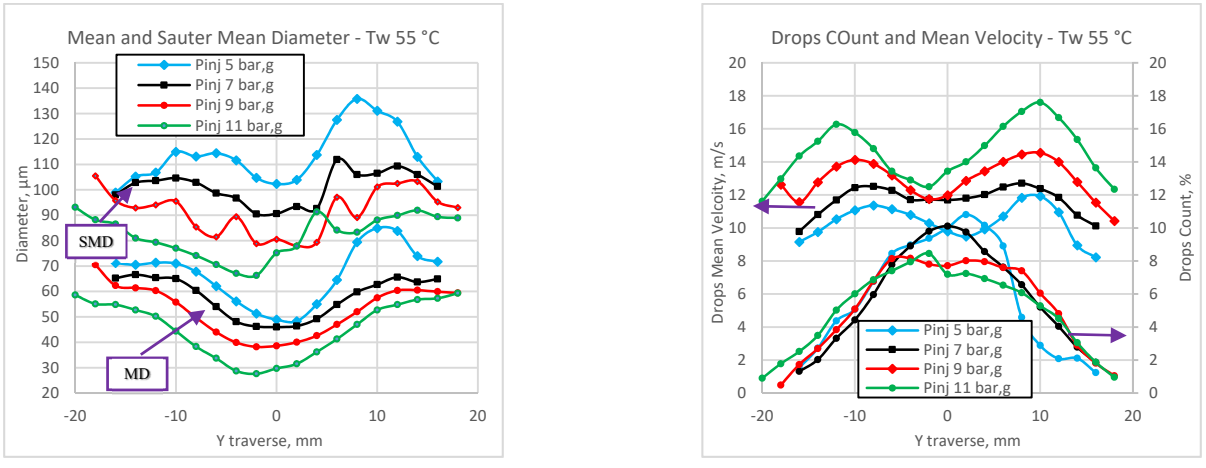

Figure 12. Effect of the injection pressure on drops' sizes and velocities over the measuring traverse at Z = 50 mm. T_w = 55 °C. (**a**) Drops' mean diameters. (**b**) Drops' counts and velocities.

Finally, in Figure 13, the diameter probability density function (PDF) for the droplet population is reported for the examined ranges of the injection pressure and water tempera-

ture. As can be observed, both the temperature and pressure variations caused a significant improvement of the atomization quality, with a consistent reduction in the PDF values for the intermediate diameter values (50–150 µm), while only marginal effects were obtained for the few very large drops produced during the initial part of the injection process. To be more detailed, it is interesting to point out how increasing the injection pressure (Figure 13b) from 5 to 11 bar,g also increased the PDF values in the range of 35–50 µm, confirming the modest atomization quality obtainable with low injection pressure values.

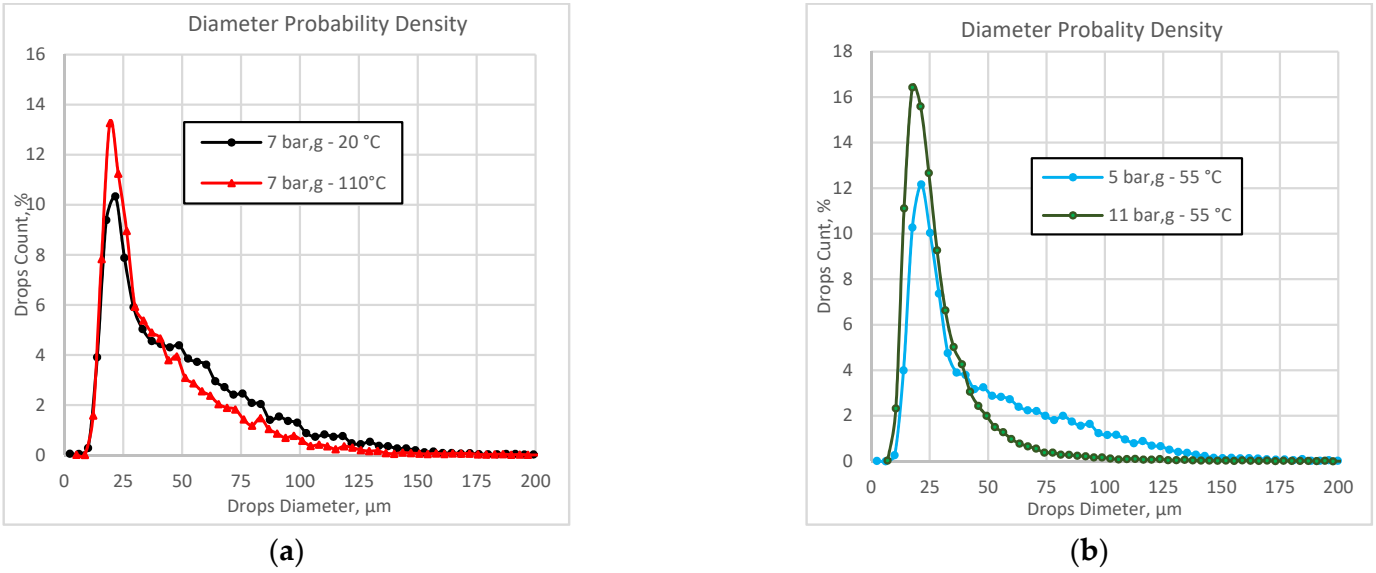

Figure 13. Effect of the injection pressure and water temperature on drops' diameter density probability functions. (**a**) P_{inj} = 7 bar,g. (**b**) T_w = 55 °C.

4. Conclusions

Water injection is promising technology for the mitigation of the knocking tendency of high-power density spark ignition engines, simplifying the adoption of high compression ratio levels and reducing the necessity for mixture enriching and spark retarding. The final goal is fully exploiting the efficiency potential of highly downsized, turbocharged spark ignition engines that have been rapidly spreading on the market in recent years.

The mixture temperature's control potential is related to the water's high latent heat of vaporization, and hence, despite the specific technology used to implement water injection, either injected directly in the combustion chamber or in the inlet runner, the water spray evaporation rate is crucial. To be more detailed, rapid and complete water spray evaporation enables controlling the mixture's temperature without significant drawbacks, such as excessive water consumption (water/fuel ratios in the range of 0.2–0.5 are quite common for full load operation) or potentially destructive lubricant oil dilution.

Port water injection (PWI) is currently considered the best compromise among system cost, complexity and efficacy. In the present paper, a deep analysis of the effects of both the water injection pressure and temperature on the resulting spray evolution and sizing characteristics was carried out separately. The ranges for both the pressure and temperature were chosen in order to be fully compliant with the low-pressure injection technology, with the water temperature and injection pressure below 110 °C and 11 bar,g, respectively. The obtained results can be summarized as follows:

- The injected mass per shot was significantly affected by the injected water's temperature. Increasing the water temperature from 20 °C to 110 °C caused a decrease of about 7% for the injected mass, depending on the injection pressure level and injection duration. This evidence seems to suggest the possible necessity of redesigning the injector coil in the case of high-temperature operation.

- In terms of the global spray evolution, no dramatic changes were observed for the spray tip penetration or cone angle in the examined injection pressure and temperature ranges which, in the present analysis, did not trigger flash boiling phenomena. Complete flash boiling development, with injection in sub-atmospheric conditions presumably not relevant for water injection operation, would require water temperature levels possibly not compatible with the standard injection components' integrity or durability.
- The spray atomization quality was sensibly affected by the water temperature's increase, with a benefit in terms of the Sauter mean diameter between 8 and 15 μm in the examined conditions. At the same time, the observed injection pressure effect was more significant, with the Sauter mean diameter reduction being approximately 20 μm and the injection pressure increasing from 5 bar,g to 11 bar,g.

The obtained results seem to confirm that there is still significant potential in the optimization of the water spray characteristics, mainly in terms of the atomization quality. To be more detailed, adequate water temperature control could assist the increase of the injection pressure in obtaining an adequate sizing level to speed up the evaporation process, contributing to water injection technology spreading.

Author Contributions: Conceptualization, L.P.; methodology, L.P. and G.B.; software, G.B.; validation, L.P., G.B. and G.M.F.; formal analysis, L.P., G.B. and G.M.F.; investigation, G.B. and G.M.F.; resources, L.P.; data curation, L.P., G.B. and G.M.F.; writing—original draft preparation, L.P.; writing—review and editing, L.P., G.B. and G.M.F.; visualization, L.P., G.B. and G.M.F.; supervision, L.P.; project administration, L.P.; funding acquisition, L.P. All authors have read and agreed to the published version of the manuscript.

Funding: This research received no external funding.

Institutional Review Board Statement: Not applicable.

Informed Consent Statement: Not applicable.

Data Availability Statement: Not applicable.

Conflicts of Interest: The authors declare no conflict of interest.

Abbreviations

GDI	Gasoline direct injection
ET	Energizing time (ms)
MD	Mean drop diameter (μm)
SMD	Sauter mean drop diameter (μm)
PDF	Probability density function
PFI	Port fuel injection
PWI	Port water injection
T_w	Water temperature (°C)
P_{inj}	Injection pressure, gauge (bar,g)

References

1. European Commission. Paris Agreement. December 2015. Available online: http://ec.europa.eu/clima/policies/international/negotiations/paris_en (accessed on 26 June 2021).
2. Commission Regulation (EU) No 459/2012 Amending Regulation (EC) No 715/2007 of the European Parliament and of the Council and Commission Regulation (EC) No 692/2008 as Regards Emissions from Light Passenger and Commercial Vehicles (Euro 6). 29 May 2012. Available online: https://eur-lex.europa.eu/legal-content/EN/TXT/?uri=celex%3A32012R0459 (accessed on 26 June 2021).
3. EEA. *Monitoring CO2 Emissions from New Passenger Cars and Vans in 2016*; EEA: Copenhagen, Denmark, 2017; ISBN 00100994.
4. Saliba, R.; Manns, J.; von Essen, C. *Groupes Motopropulseurs du Futur pour une Mobilité à faibles Émissions de Carbone*; CNAM: Paris, France, 2018.
5. Zhao, H. *Advanced Direct Injection Combustion Engine Technologies and Development: Gasoline Engines*; Elsevier: Amsterdam, The Netherlands, 2009; Volume 1.
6. Johnson, T.; Joshi, A. Review of Vehicle Engine Efficiency and Emissions. *SAE Int. J. Engines* **2018**, *11*, 1307–1330. [CrossRef]

7. Zhu, S.; Hu, B.; Akehurst, S.; Copeland, C.; Lewis, A.; Yuan, H.; Kennedy, I.; Bernards, J.; Branney, C. A review of water injection applied on the internal combustion engine. *Energy Convers. Manag.* **2019**, *184*, 139–158. [CrossRef]
8. Millo, F.; Mirzaeian, M.; Rolando, L.; Bianco, A.; Postrioti, L. A methodology for the assessment of the knock mitigation potential of a port water injection system. *Fuel* **2021**, *283*, 119251. [CrossRef]
9. Iacobacci, A.; Marchitto, L.; Valentino, G. Water Injection to Enhance Performance and Emissions of a Turbocharged Gasoline Engine under High Load Condition. *SAE Int. J. Engines* **2017**, *10*, 928–937. [CrossRef]
10. Cordier, M.; Lecompte, M.; Malbec, L.-M.; Reveille, B.; Servant, C.; Souidi, F.; Torcolini, N. Water Injection to Improve Direct Injection Spark Ignition Engine Efficiency. *SAE Tech. Pap.* **2019**. [CrossRef]
11. Gern, M.S.; Vacca, A.; Bargende, M. Experimental Analysis of the Influence of Water Injection Strategies on DISI Engine Particle Emissions. *SAE Int. J. Adv. Curr. Prac. Mobil.* **2020**, *2*, 598–606. [CrossRef]
12. Paltrinieri, S.; Mortellaro, F.; Silvestri, N.; Rolando, L.; Medda, M.; Corrigan, D. Water Injection Contribution to Enabling Stoichiometric Air-to-Fuel Ratio Operation at Rated Power Conditions of a High-Performance DISI Single Cylinder Engine. *SAE Tech. Pap.* **2019**. [CrossRef]
13. Cavina, N.; Rojo, N.; Businaro, A.; Brusa, A.; Corti, E.; De Cesare, M. Investigation of Water Injection Effects on Combustion Characteristics of a GDI TC Engine. *SAE Int. J. Engines* **2017**, *10*, 2209–2218. [CrossRef]
14. Khatri, J.; Denbratt, I.; Dahlander, P.; Koopmans, L. Water Injection Benefits in a 3-Cylinder Downsized SI-Engine. *SAE Int. J. Adv. Curr. Prac. Mobil.* **2019**, *1*, 236–248. [CrossRef]
15. Falfari, S.; Bianchi, G.M.; Cazzoli, G.; Ricci, M.; Forte, C. Water Injection Applicability to Gasoline Engines: Thermodynamic Analysis. *SAE Tech. Pap.* **2019**. [CrossRef]
16. Berni, F.; Breda, S.; Lugli, M.; Cantore, G. A Numerical Investigation on the Potentials of Water Injection to Increase Knock Resistance and Reduce Fuel Consumption in Highly Downsized GDI Engines. *Energy Proc.* **2015**, *81*, 826–835. [CrossRef]
17. Hoppe, F.; Thewes, M.; Seibel, J.; Balazs, A.; Scharf, J. Evaluation of the Potential of Water Injection for Gasoline Engines. *SAE Int. J. Engines* **2017**, *10*, 2500–2512. [CrossRef]
18. Sun, Y.; Fischer, M.; Bradford, M.; Kotrba, A.; Randolph, E. Water Recovery from Gasoline Engine Exhaust for Water Injection. *SAE Tech. Pap.* **2018**. [CrossRef]
19. Yasukawa, Y.; Okamoto, Y.; Kobayashi, N.; Saito, T.; Saruwatari, M. Multi-Swirl Type Injector for Port Fuel Injection Gasoline Engines. *SAE Tech. Pap.* **2014**. [CrossRef]
20. Van Vuuren, N.; Postrioti, L.; Brizi, G.; Picchiotti, F. Instantaneous Flow Rate Testing with Simultaneous Spray Visualization of an SCR Urea Injector at Elevated Fluid Temperatures. *SAE Int. J. Engines* **2017**, *10*, 2478–2485. [CrossRef]
21. Kapusta, Ł.J.; Rogoz, R.; Bachanek, J.; Boruc, Ł.; Teodorczyk, A. Low-Pressure Injection of Water and Urea-Water Solution in Flash-Boiling Conditions. *SAE Int. J. Adv. Curr. Prac. Mobil.* **2021**, *3*, 365–377. [CrossRef]
22. Postrioti, L.; Caponeri, G.; Buitoni, G.; van Vuuren, N. Experimental Assessment of a Novel Instrument for the Injection Rate Measurement of Port Fuel Injectors in Realistic Operating Conditions. *SAE Int. J. Fuels Lubr.* **2017**, *10*, 344–351. [CrossRef]
23. Brizi, G.; Postrioti, L.; van Vuuren, N. Experimental Analysis of SCR Spray Evolution and Sizing in High-Temperature and Flash Boiling Conditions. *SAE Int. J. Fuels Lubr.* **2019**, *12*, 87–108. [CrossRef]
24. Postrioti, L.; Malaguti, S.; Bosi, M.; Buitoni, G.; Piccinini, S.; Bagli, G. Experimental and numerical characterization of a direct solenoid actuation injector for Diesel engine applications. *Fuel* **2014**, *118*, 316–328. [CrossRef]
25. Postrioti, L.; Ubertini, S. An integrated experimental-numerical study of HSDI Diesel injection system and spray dynamics. *SAE Tech. Pap.* **2006**. [CrossRef]